Elastic softening and hardening at intersections between twin walls and surfaces in ferroelastic materials

Xiaomei He, Xiangdong Ding, Jun Sun, Guillaume F Nataf, Ekhard K H Salje

Elastic softening and hardening at intersections between twin walls and surfaces in ferroelastic materials

Xiaomei He[1,2], Xiangdong Ding[1,*], Jun Sun[1] , Guillaume F. Nataf[3], and Ekhard K. H. Salje[1,4*]

[1] State Key Laboratory for Mechanical Behavior of Materials, Xi'an Jiaotong University, Xi'an 710049, China

[2] State Key Laboratory for Strength and Vibration of Mechanical Structures, Department of Engineering Mechanics, Xi'an Jiaotong University, Xi'an 710049, China

[3] GREMAN UMR7347, CNRS, University of Tours, INSA Centre Val de Loire, 37000 Tours, France

[4] Department of Earth Sciences, University of Cambridge, Downing Street, Cambridge CB23EQ, UK

E-mail: dingxd@mail.xjtu.edu.cn; ekhard@esc.cam.ac.uk

ABSTRACT

Surfaces play a key role during ferroelastic switching and define the interactions of materials with ionic species and biological systems. Here, we perform molecular dynamics simulations and identify ridges and valleys with rounded singularities around the intersections between twin walls and surfaces. Two dominant length scales stem from the elastic bending of the surface layer (> 30 lattice units) and local atomic reshuffles (some 5 lattice units). For static twin walls, which do not shift laterally under external stress, the intrinsic change of the Young's modulus involves softening near valleys and hardening near ridges. The boundary-induced changes of the surface Young's modulus are in the order of 0.7%.

Keywords:
Elastic softening; Ferroelastic materials; Wall-surface intersections; Surface relaxations

INTRODUCTION

Twin boundaries (TBs, also named twin walls or domain walls) are only a few nanometers thick and form large sheets embedded in the bulk material. Their studies in ferroelastic materials have greatly expanded over the last years since it is understood that they can be used as templates for a large group of multiferroic device.[1-3] The rational is that twin walls have intrinsically different properties compared to the bulk material. Wall related properties range from altered electronic properties,[4-6] localized superconductivity,[6] and chemical changes,[7,8] to local magnetism and magnetoelectric coupling in multiferroics.[9,10] The properties of twin walls are particularly sensitive to external perturbations, such as light illumination, electric and magnetic fields.[11-13] Their potential for the use as high density memory storage includes either direct local switching[14] or collective switching of ferroelastic Bloch-lines.[15]

Since twin walls are topologically protected, they cannot simply terminate in the bulk material. Instead, they either combine with another twin wall to form a needle domain,[16] bend to combine with the other end of the wall and form a bubble domain, or propagate until they encounter the sample surface. Surfaces pin twin walls and greatly influence their sideways movement.[17-23] At the surface, Landau-Ginzburg-based models predict that twin walls exhibit a double-peak elastic strain and wedge-shaped topography,[24] as confirmed by numerical simulations.[25,26] The resulting elastic fields decrease locally the electronic band gap and lead to an enhanced electric conductivity.[27] They also induce polarity in otherwise non-polar bulk materials.[28]

While the surface deformation is rather well understood there is yet no fundamental understanding of the elastic properties of these surface structures near the intersection lines. This is mostly because it is experimentally challenging to isolate the mechanical response of an individual wall with nanometric thickness, without getting a response dominated by the surrounding domains. Interestingly, the rare mechanical measurements performed on non-ferroelastic 180° domain walls reveal an unexpected behaviour, with a domain wall softening.[29-31] In ferroelastics, the elastic response is determined by two different processes: either the penetrating twin walls move, or they do not move. Moving twin walls always soften materials and are part of the ferroelastic character of the material.[32-34] However, static twin walls are a 'true' intrinsic surface property. Their investigation has largely eluded theoretical and experimental studies. In a recent

work, Nguyen *et al.*[35] investigated the nanomechanical properties of 90° walls of $PbTiO_3$, i.e. twin walls, by using atomic force microscopy methods. They found considerable changes of the elastic moduli at the intersection lines extending up to ~100 nm into the domain areas.

Here, we focus on purely ferroelastic materials, where nonlinear elastic interactions dominate the intersections between twin walls and surfaces on several characteristic length scales.[28,32] We perform molecular dynamics (MD) simulations of a ferroelastic surface where twin walls produce ridges and valleys. We then compute the strain profile, elastic modulus, and elastic compliance of twin walls near the surfaces.

METHODS

Our molecular dynamic simulations are based on a sandwich model with nonlinear elastic interactions. The interaction potentials are described in refs. 36,37 with first-NN harmonic interaction $U_{1st\text{-}NN} = 2(r-1)^2$, $0.8 \le r < 1.2$, second-NN Landau spring interaction $U_{2nd\text{-}NN} = -(r-\sqrt{2})^2 + 200\ (r-\sqrt{2})^4$, $1.207 \le r < 1.621$, and third-NN fourth-order interaction $U_{3rd\text{-}NN} = -0.1(r-2)^4$, $1.8 \le r < 2.2$, where r is the interatomic distance vector. The ferroelastic shear is 4°,[38,39] the lattice parameters a_0 and b_0 are set to 1 lattice unit for the initial model at 0 K, and atomic mass is 1 amu. The complete sample cell is $600a_0 \times 302b_0$ (Fig. 1). Twin boundaries along [100] at Y = 0 and Y=101 are denoted TB1 and TB2. Direct interactions between TB1 and TB2 are avoided by large interwall distances. The twin angles have opposite signs in TB1 and TB2. Each TB intersects the surface at a ridge or a valley. In Fig.1, TB1 shows a valley configuration (TB1-Valley) and TB2 shows a ridge (TB2-Ridge) at the left surface. In contrast, TB1 shows a ridge (TB1-Ridge) and TB2 shows a valley (TB2-Valley) at the right surface. Open boundary conditions are applied in both x and y directions. The sample was relaxed at a very low temperature ($10^{-7}\ T_C$) to avoid thermal noise. T_C (~12.5 K) is the ferroelastic phase transition of this model. The relaxation generates surface strain at the valley and ridge intersection sites. Once the sample is relaxed to a residual strain ~3×10^{-7}, we applied the spring forces at the left and right surfaces with a spring constant of ~10 N/m to compress the sample. The magnitude of the force induced displacements is sufficiently low to ensure that the level of compression remains within the elastic range. We increased the compressive force over 1.5×10^7 time-steps with a residual random strain ~7×10^{-7} in the bulk (i.e.,

the 'noise' of the simulation). The simulations were performed using the LAMMPS code.[40] Canonical (NVT) ensemble was used and the temperature of the sample was held by a Nosé-Hoover thermostat.[41] Atomic images were visualized by the OVITO code.[42]

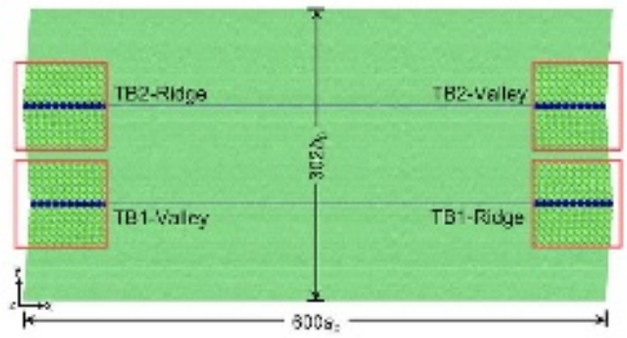

FIG. 1. The ferroelastic model has two horizontal twin boundaries (TB1 and TB2). The frames mark the ridge and valley intersections at the surfaces for both TB1 and TB2.

RESULTS AND DISCUSSION

Figure 2 shows the distribution of the strain components near the intersections. The strains ε_{xx}, ε_{yy} and ε_{xy} are defined with respect to the bulk:

$$\varepsilon_{xx}(N_x, \mathrm{Y}) = (a(N_x, \mathrm{Y}) - a_{\mathrm{bulk}}) / a_{\mathrm{bulk}}\,, \tag{1}$$

$$\varepsilon_{yy}(\mathrm{X}, N_y) = (b(\mathrm{X}, N_y) - b_{\mathrm{bulk}}) / b_{\mathrm{bulk}}\,, \tag{2}$$

$$\varepsilon_{xy}(N_x, N_y) = (|\tfrac{\Delta\gamma}{b}|(N_x, N_y) - |\tfrac{\Delta\gamma}{b}|_{\mathrm{bulk}}) / |\tfrac{\Delta\gamma}{b}|_{\mathrm{bulk}}\,, \tag{3}$$

where N_x is the layer number in x direction, N_y is the layer number in y direction, a and b are the averaged bulk lattice repetition units in x and y direction, $\Delta\gamma$ is the shear deformation in a lattice cell along the x direction, and $|\frac{\Delta\gamma}{b}|(N_x,N_y)$ is the shear strain.

The atomic configurations are color-coded by ε_{xx}, ε_{yy}, and ε_{xy} in Fig. 2(a)-(c). The corresponding strain profiles are shown in Fig. 2(d)-(f). Surface layers show surface relaxations with compression in x. Weak tensile strain (red regions in Fig. 2(a)) develops near the twin wall, mainly due to the inclination of the surface of the twin configurations with respect to the tensile force. The expansion or compression of surface relaxations depends on the ratio between the first- and second-neighbour interactions.[43] In our model, the second-neighbour attraction overcomes the first-neighbour repulsion with $\varepsilon_{xx}<0$ at the surface layers. ε_{xy} changes sign in the twin wall. The averaged shear

angle in the bulk is θ_{ave} =3.9922°, which is slightly smaller than 4° of the single domains. ε_{xy} near the ridge is larger than in the bulk with higher shear angles than θ_{ave} and very close to 4° (Fig. 2(f)). In contrast, ε_{xy} is smaller near the valley with shear angles below θ_{ave}. The strain profiles agree well with linear elasticity models which predicted a double-peak elastic strain and wedge-shaped topography in the surface.[26]

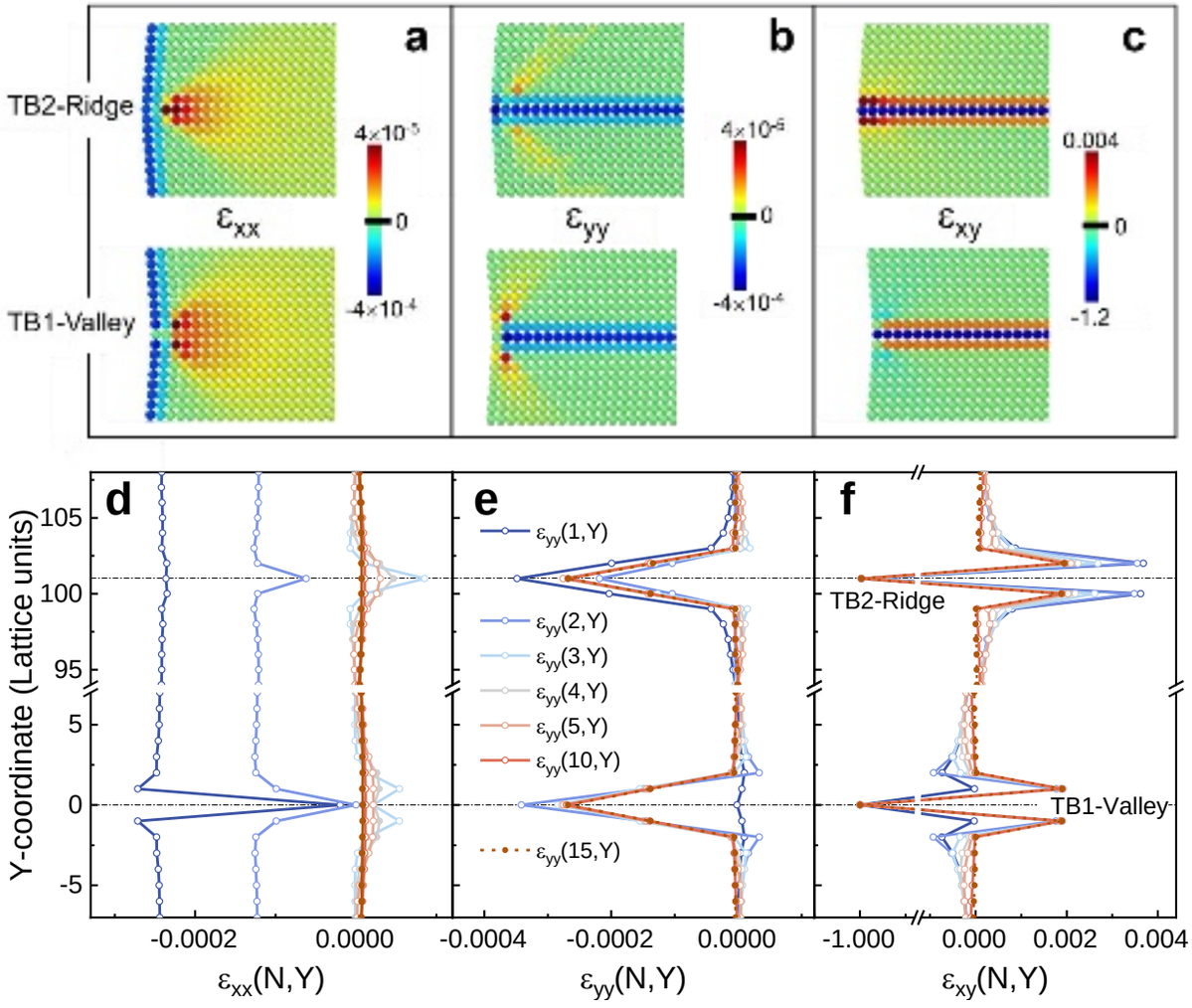

FIG. 2. Strain profiles of intersections between twin boundaries and the surfaces forming valleys (TB1-Valley) and ridges (TB2-Ridge). (a)-(c) are the atomic images color-coded according to the strain components of ε_{xx}, ε_{yy} and ε_{xy}, respectively. (d)-(f) presents the strain profiles from the 1st layer to the 15th layer near the surface.

Opposing spring forces are applied to both surfaces. The force induced elastic displacements are less than 1×10^{-4} lattice units at 1 lattice unit to maintain the deformation within the elastic range.

Force (F) induced deformation yields surface shifts within a range from 0.0008 lattice units (F = 7.68 × 10^{-4} nN) to 0.03 lattice units (F = 2.88 × 10^{-2} nN) are calculated. With F = 7.68 × 10^{-4} nN, as an example, the force induced atomic images and surface layer shifts Δx are shown in Fig. 3. The blue arrows in Fig. 3(a) show the displacement vectors of surface atoms from their original positions (without external force) to the new force induced equilibrium positions. The atoms near the core of the ridge (Y=101) shift less while the shift increased with the atom distance away from Y=101. The atoms at the core of the valley (Y=0) show the largest shift. Δx exponentially decays from the core intersection to interlayers along the y direction and saturates after 40-50 layers (Fig. 3(b)). Force induced shear angle difference $\Delta\theta$, relative to the initial state after relaxation, is shown in Fig. 3(c). $\Delta\theta$ exponentially decays from ridge and valley sites and extends over 25-30 lattice units.

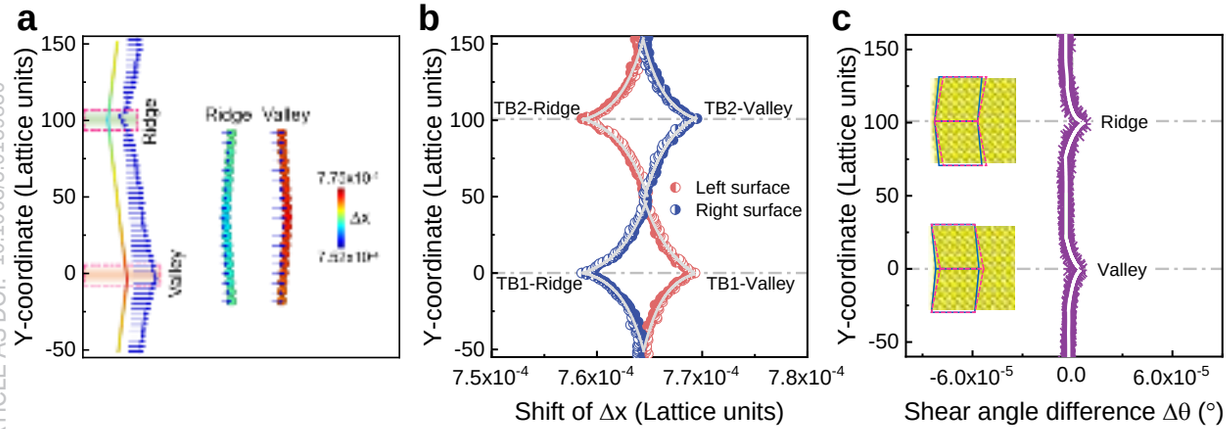

FIG. 3. Force-induced (a) surface layer atomic topology, (b) shift of the surface layers along [100] at the left surface and along [$\bar{1}$00] at the right surface, and (c) shear angle difference relative to the initial state after relaxation. The dotted red areas in (a) are enlarged with colours coded by the magnitude of the shifts Δx (in lattice units). Arrow vectors are amplified by a factor of 6000 for clarity. The shift profiles in (b) decay exponentially with increasing distance from the TB in vertical y direction.

The Young's modulus is $E_{[100]} = Fa(1,Y)/(S\varepsilon_{[100]})$, with force F = 5.76 × 10^{-4} nN , surface S of the (100) plane, interatomic distances $a(1,Y)$ near the surface and lattice strain $\varepsilon_{[100]}$. The elastic compliance is $S_{11} = 1/E_{[100]}$ in this pseudo cubic setting. Figure 4 shows the Young's modulus and the compliance profiles of the surface layer. The Young's modulus at the intersection centre is

$E_{[100]}^{valley}$ = 100.04 GPa and $E_{[100]}^{ridge}$ = 101.44 GPa. They deviate by ca. 0.7% from the undisturbed surface $E_{[100]}^{bulk}$ = 100.73 GPa. This result confirms softening of valleys and hardening of ridges.

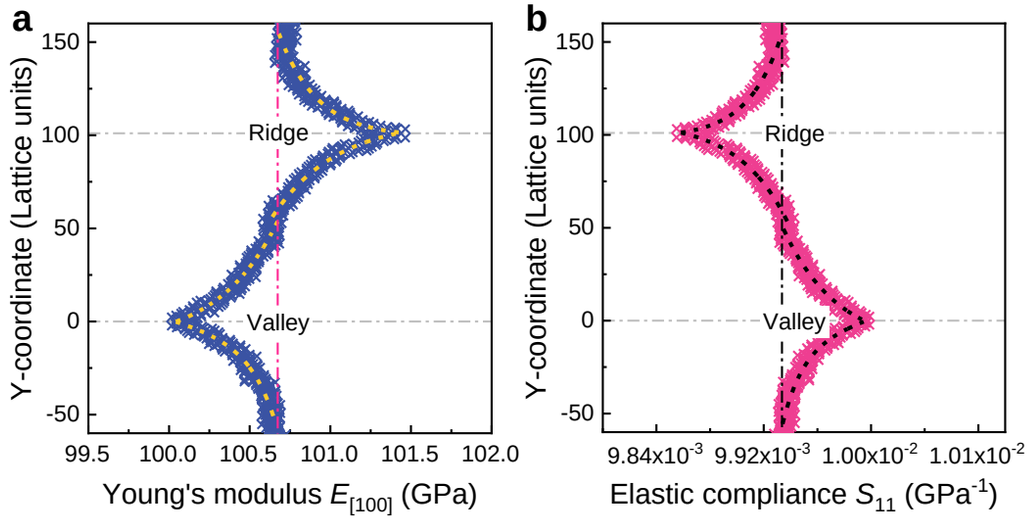

FIG. 4. The profiles of (a) elastic modulus and (b) elastic compliance of the surface layer. Softening of moduli at the valley and hardening at the ridge are observed.

The surface strain has a significant fine structure near the twin wall. While simple twin domains would lead to a sharp break where the surfaces are inclined with opposite tilt angles, this singularity is smoothed by relaxations.[26,44,45] The long length scale describes an exponential decay which extends in our model simulations over some 30 lattice units on both sides of the twin wall (Fig. 3(b)). The second relaxation is limited to the thickness of the twin wall which extends over 5 lattice units (Fig. 2), and hosts potentially novel structural states with interesting physical properties [1–3]. The strains are < 2×10^{-4} in ε_{xx} and ε_{yy} and extend to the full spontaneous strain in ε_{xy}. Experimentally, the twin walls are often wider and can be as large as 20 nm[46,47] so that our estimation may be smaller than that in real ferroelastic materials.

The results in Fig. 4 show that the moduli are indeed constant inside each twin domain but deviate near the intersection sites. Our main result is that ridges and valleys show opposite tendencies: ridges harden, and valleys soften. The moduli decay from the middle of the intersection approximately exponentially over some 30 lattice units. In perovskite structures with ca. 0.5 nm lattice repetition lengths, this elastic decay would extend over some 15 nm on each side of the wall. The hard or soft region is then some 30 nm wide. The apparent half width of the softening at the

wall measured in lead zirconate titanate by Tsuji *et al.* [29] extended on 20–30 nm, but was probably widened due to the diameter of the tip. Stefani *et al.* [31] studied the mechanical softness of ferroelectric domain walls in $LiNbO_3$ and $BaTiO_3$ by atomic force microscopy and found softened regions of ~60 nm.

The simulated change of the Young's modulus is around 0.7%. Elastic modulus orthogonal to the averaged surface can be measured by atomic force microscopy or by indentation tests. However, in most experiments, the external force moves the intersection laterally away from the singularity and one observes an apparent softening even when the intrinsic response is hardening (as commonly observed in bulk ferroelastics with moving twin walls[32-34]). The elastic modulus softening measured in lead zirconate titanate[29] was significantly higher than in our simulations with more than 12% reduction. Recently, domain wall softening of $BaTiO_3$ at short-circuit boundary conditions with/without shear piezoelectricity was studied by Stefani *et al.* [31]. They observed domain wall softening reduced from 6% to 0.3% after removal of the shear piezoelectricity effect. This illustrates that depolarization-activated electromechanical coupling effects would produce an additional softening. Temperature is expected to change the magnitude of the modulus anomaly, further work to explore the temperature dependence is in progress.

In ref. 35, they confirmed the predicted long length scale of 100 nm while the investigation of the short length scale was beyond the possibilities of their atomic force microscopy-based measurements. The ridge twin wall was found to have the lowest elastic modulus while the valley wall had the highest value, contrary to our simulations. This may be induced by several factors in the experiment: the twin walls are not vertical but are tilted by 45° to the surface, the twin walls likely host defects that could change the mechanical properties,[48,49] there might be a contribution from the topography. Furthermore, in our geometrical configurations we have chosen to have the same modulus in both adjacent domains.

Another possible source of different results stems from the most fundamental property of the intersection lines because they can bend and, most importantly, move laterally during the experiment. To avoid this effect materials should be analysed where the twin walls are very firmly pinned. A typical case is $CaTiO_3$ while $PbTiO_3$ shows particularly mobile walls. The 'true' intrinsic elastic response of these materials may be rather different depending on the local mobility of the twin walls under stress.

CONCLUSIONS

We performed molecular dynamic simulations of a ferroelastic surface where twin walls produce ridges and valleys. We find that the Young's modulus involves softening near valleys and hardening near ridges with changes in the order of 0.7%. The moduli decay from the middle of the intersection approximately exponentially over some 30 lattice units, in agreement with experimental results in the literature. This proves that ferroelectric/ferroelastic twin walls at surface intersections are far from being simple superpositions of elastic properties of the surfaces and the wall relaxations.[25,37,44,50] Our theoretical analysis of this mechanical fine structure will help future atomic force microscopy and indentation studies[51,52] to compare their results with our predicted elastic anomalies.

Our results point also to many potential applications. Regions with different Young's moduli will locally affect phonon velocities and change thermal conductivity.[53] As such the softening and hardening of twin walls could explain their influence on thermal conductivity[54,55] and lead to devices with different thermal conductivities near the surface and in the bulk. When twin walls are fast ionic conductors,[56,57] the surface intersections constitute the exchange regions between the wall diffusion and the external sources so that ionic injections are only possible if they are not blocked at the sites. This is a major issue in neuromorphic computation[58] and specific surface configurations are often needed in such applications. For instance, it is known that variations in Young's modulus influence the ionic conductivity of solid electrolytes.[59] In a different field, biogenetic processes often proceed along surfaces and are known to be affected by the surface topology. In particular, the stiffness of the surface is a critical parameter: bacterial adhesion is found to depend on the material stiffness regardless of hydrogel chemistry or adhesion mechanism.[60] In ferroelastic materials, not only the surface topology depends on the intersection lines but also the elastic response. The soft and hard region in valleys and ridges will presumably have very different attachment potentials and will structure the biological processes along ferroelastic domain patterns.[60]

DECLARATIONS

Availability of data

The data that support the findings of this study are available from the corresponding author upon reasonable request.

Financial support

This work was supported by the National Key Research and Development Program of China (2019YFA0307900). X.D. and J.S. acknowledge support from the National Natural Science Foundation of China (51931004) and 111 project 2.0 (BP2018008). E.K.H.S. is grateful to EPSRC (EP/P024904/1) and the EU's Horizon 2020 program under the Marie Sklodowska-Curie Grant (grant number 861153).

Conflicts of interest

The authors have no conflicts to disclose.

REFERENCES

[1] E. K. H. Salje, *Multiferroic Domain Boundaries as Active Memory Devices: Trajectories Towards Domain Boundary Engineering*, ChemPhysChem **11**, 940 (2010).

[2] G. F. Nataf, M. Guennou, J. M. Gregg, D. Meier, J. Hlinka, E. K. H. Salje, and J. Kreisel, *Domain-Wall Engineering and Topological Defects in Ferroelectric and Ferroelastic Materials*, Nat. Rev. Phys. **2**, 634 (2020).

[3] D. Meier and S. M. Selbach, *Ferroelectric Domain Walls for Nanotechnology*, Nat. Rev. Mater. **7**, 157 (2021).

[4] J. Seidel et al., *Conduction at Domain Walls in Oxide Multiferroics.*, Nat. Mater. **8**, 229 (2009).

[5] P. S. Bednyakov, B. I. Sturman, T. Sluka, A. K. Tagantsev, and P. V. Yudin, *Physics and Applications of Charged Domain Walls*, npj Comput. Mater. **4**, 65 (2018).

[6] A. Aird and E. K. H. Salje, *Sheet Superconductivity in Twin Walls: Experimental Evidence of WO_{3-x}*, J. Phys. Condens. Matter **10**, L377 (1998).

[7] E. K. H. Salje and S. Kustov, *Dynamic Domain Boundaries: Chemical Dopants Carried by Moving Twin Walls*, Phys. Chem. Chem. Phys. **25**, 1588 (2023).

[8] S. Farokhipoor et al., *Artificial Chemical and Magnetic Structure at the Domain Walls of an Epitaxial Oxide*, Nature **515**, 379 (2014).

[9] Y. Geng, N. Lee, Y. J. Choi, S.-W. Cheong, and W. Wu, *Collective Magnetism at Multiferroic Vortex Domain Walls*, Nano Lett. **12**, 6055 (2012).

[10] M. Giraldo, Q. N. Meier, A. Bortis, D. Nowak, N. A. Spaldin, M. Fiebig, M. C. Weber, and T. Lottermoser, *Magnetoelectric Coupling of Domains, Domain Walls and Vortices in a Multiferroic with Independent Magnetic and Electric Order*, Nat. Commun. **12**, 3093 (2021).

[11] F. Rubio-Marcos, A. Del Campo, P. Marchet, and J. F. Fernández, *Ferroelectric Domain Wall Motion Induced by Polarized Light*, Nat. Commun. **6**, 6594 (2015).

[12] J. Schaab et al., *Electrical Half-Wave Rectification at Ferroelectric Domain Walls*, Nat. Nanotechnol. **13**, 1028 (2018).

[13] E. Hassanpour et al., *Interconversion of Multiferroic Domains and Domain Walls*, Nat. Commun.

12, 2755 (2021).

[14] P. Sharma, Q. Zhang, D. Sando, C. H. Lei, Y. Liu, J. Li, V. Nagarajan, and J. Seidel, *Nonvolatile Ferroelectric Domain Wall Memory*, Sci. Adv. **3**, e1700512 (2017).

[15] E. K. H. Salje and J. F. Scott, *Ferroelectric Bloch-Line Switching: A Paradigm for Memory Devices?*, Appl. Phys. Lett. **105**, 252904 (2014).

[16] E. K. H. Salje and Y. Ishibashi, *Mesoscopic Structures in Ferroelastic Crystals: Needle Twins and Right-Angled Domains*, J. Phys. Condens. Matter **8**, 8477 (1996).

[17] P. Gao et al., *Ferroelastic Domain Switching Dynamics under Electrical and Mechanical Excitations*, Nat. Commun. **5**, 3801 (2014).

[18] G. Lu, S. Li, X. Ding, J. Sun, and E. K. H. Salje, *Electrically Driven Ferroelastic Domain Walls, Domain Wall Interactions, and Moving Needle Domains*, Phys. Rev. Mater. **3**, 114405 (2019).

[19] J. Y. Jo, S. M. Yang, T. H. Kim, H. N. Lee, J.-G. Yoon, S. Park, Y. Jo, M. H. Jung, and T. W. Noh, *Nonlinear Dynamics of Domain-Wall Propagation in Epitaxial Ferroelectric Thin Films*, Phys. Rev. Lett. **102**, 045701 (2009).

[20] A. Gruverman, B. J. Rodriguez, R. J. Nemanich, and A. I. Kingon, *Nanoscale Observation of Photoinduced Domain Pinning and Investigation of Imprint Behavior in Ferroelectric Thin Films*, J. Appl. Phys. **92**, 2734 (2002).

[21] Y. Kim, M. Alexe, and E. K. H. Salje, *Nanoscale Properties of Thin Twin Walls and Surface Layers in Piezoelectric WO_{3-x}*, Appl. Phys. Lett. **96**, 032904 (2010).

[22] R. Jarrier et al., *Surface Phase Transitions in $BiFeO_3$ below Room Temperature*, Phys. Rev. B **85**, 184104 (2012).

[23] L. Zhang, S. Li, X. Ding, J. Sun, and E. K. H. Salje, *Statistical Analysis of Emission, Interaction and Annihilation of Phonons by Kink Motion in Ferroelastic Materials*, Appl. Phys. Lett. **116**, 102902 (2020).

[24] J. Novak and E. K. H. Salje, *Simulated Mesoscopic Structures of a Domain Wall in a Ferroelastic Lattice*, Eur. Phys. J. B **4**, 279 (1998).

[25] J. Novak and E. K. H. Salje, *Surface Structure of Domain Walls*, J. Phys. Condens. Matter **10**, L359 (1998).

[26] S. Conti and E. K. H. Salje, *Surface Structure of Ferroelastic Domain Walls: A Continuum Elasticity Approach*, J. Phys. Condens. Matter **13**, L847 (2001).

[27] E. A. Eliseev, A. N. Morozovska, Y. Gu, A. Y. Borisevich, L.-Q. Chen, V. Gopalan, and S. V. Kalinin, *Conductivity of Twin-Domain-Wall/Surface Junctions in Ferroelastics: Interplay of Deformation Potential, Octahedral Rotations, Improper Ferroelectricity, and Flexoelectric Coupling*, Phys. Rev. B **86**, 085416 (2012).

[28] Z. Zhao, N. Barrett, Q. Wu, D. Martinotti, L. Tortech, R. Haumont, M. Pellen, and E. K. H. Salje, *Interaction of Low-Energy Electrons with Surface Polarity near Ferroelastic Domain Boundaries*, Phys. Rev. Mater. **3**, 043601 (2019).

[29] T. Tsuji, S. Saito, K. Fukuda, K. Yamanaka, H. Ogiso, J. Akedo, and Y. Kawakami, *Significant Stiffness Reduction at Ferroelectric Domain Boundary Evaluated by Ultrasonic Atomic Force Microscopy*, Appl. Phys. Lett. **87**, 071909 (2005).

[30] T. Tsuji, H. Ogiso, J. Akedo, S. Saito, K. Fukuda, and K. Yamanaka, *Evaluation of Domain Boundary of Piezo/Ferroelectric Material by Ultrasonic Atomic Force Microscopy*, Jpn. J. Appl. Phys. **43**, 2907 (2004).

[31] C. Stefani, L. Ponet, K. Shapovalov, P. Chen, E. Langenberg, D. G. Schlom, S. Artyukhin, M.

Stengel, N. Domingo, and G. Catalan, *Mechanical Softness of Ferroelectric 180° Domain Walls*, Phys. Rev. X **10**, 041001 (2020).

[32] E. K. H. Salje, *Ferroelastic Materials*, Annu. Rev. Mater. Res. **42**, 265 (2012).

[33] W. Schranz and A. V. Kityk, *Domain Wall Dynamics in Ferroelastic Crystals*, Ferroelectrics **375**, 178 (2008).

[34] W. Schranz, H. Kabelka, A. Sarras, and M. Burock, *Giant Domain Wall Response of Highly Twinned Ferroelastic Materials*, Appl. Phys. Lett. **101**, 141913 (2012).

[35] C. T. Nguyen, P. Schoenherr, and J. Seidel, *Intrinsic Mechanical Compliance of 90° Domain Walls in $PbTiO_3$*, Adv. Funct. Mater. **33**, 2211906 (2023).

[36] E. K. H. Salje, X. Wang, X. Ding, and J. F. Scott, *Ultrafast Switching in Avalanche-driven Ferroelectrics by Supersonic Kink Movements*, Adv. Funct. Mater. **27**, 1700367 (2017).

[37] X. He, S. Li, X. Ding, J. Sun, S. Kustov, and E. K. H. Salje, *Internal Friction in Complex Ferroelastic Twin Patterns*, Acta Mater. **228**, 117787 (2022).

[38] R. Harrison, S. Redfern, and E. Salje, *Dynamical Excitation and Anelastic Relaxation of Ferroelastic Domain Walls in $LaAlO_3$*, Phys. Rev. B **69**, 144101 (2004).

[39] S. Van Aert, S. Turner, R. Delville, D. Schryvers, G. Van Tendeloo, and E. K. H. Salje, *Direct Observation of Ferrielectricity at Ferroelastic Domain Boundaries in $CaTiO_3$ by Electron Microscopy*, Adv. Mater. **24**, 523 (2012).

[40] S. Plimpton, *Fast Parallel Algorithms for Short-Range Molecular Dynamics*, J. Comput. Phys. **117**, 1 (1995).

[41] S. Nosé, *A Unified Formulation of the Constant Temperature Molecular Dynamics Methods*, J. Chem. Phys. **81**, 511 (1984).

[42] A. Stukowski, *Visualization and Analysis of Atomistic Simulation Data with OVITO–the Open Visualization Tool*, Model. Simul. Mater. Sci. Eng. **18**, 015012 (2010).

[43] B. Houchmandzadeh, J. Lajzerowicz, and E. Salje, *Relaxations near Surfaces and Interfaces for First-, Second- and Third-Neighbour Interactions: Theory and Applications to Polytypism*, J. Phys. Condens. Matter **4**, 9779 (1992).

[44] M. Alexe, C. Harnagea, D. Hesse, and U. Gösele, *Polarization Imprint and Size Effects in Mesoscopic Ferroelectric Structures*, Appl. Phys. Lett. **79**, 242 (2001).

[45] W. T. Lee, E. K. H. Salje, and U. Bismayer, *Domain-Wall Structure and Domain-Wall Strain*, J. Appl. Phys. **93**, 9890 (2003).

[46] S. Yun, K. Song, K. Chu, S.-Y. Hwang, G.-Y. Kim, J. Seo, C.-S. Woo, S.-Y. Choi, and C.-H. Yang, *Flexopiezoelectricity at Ferroelastic Domain Walls in WO_3 Films*, Nat. Commun. **11**, 4898 (2020).

[47] W. Lee, E. K. H. Salje, and U. Bismayer, *Influence of Point Defects on the Distribution of Twin Wall Widths*, Phys. Rev. B **72**, 104116 (2005).

[48] Y. Liu, Y.-L. Tang, Y.-L. Zhu, W.-Y. Wang, and X.-L. Ma, *Spatial Coupling of Ferroelectric Domain Walls and Crystallographic Defects in the $PbTiO_3$ Films*, Adv. Mater. Interfaces **3**, 1600342 (2016).

[49] A. Chandrasekaran, D. Damjanovic, N. Setter, and N. Marzari, *Defect Ordering and Defect – Domain-Wall Interactions in $PbTiO_3$: A First-Principles Study*, **88**, 1 (2013).

[50] J. Chrosch and E. K. H. Salje, *Near-Surface Domain Structures in Uniaxially Stressed*, J. Phys. Condens. Matter **10**, 2817 (1998).

[51] S. V. Kalinin, A. Gruverman, B. J. Rodriguez, J. Shin, A. P. Baddorf, E. Karapetian, and M. Kachanov, *Nanoelectromechanics of Polarization Switching in Piezoresponse Force Microscopy*, J.

Appl. Phys. **97**, 074305 (2005).

[52] N. X. Randall, M. Vandamme, and F.-J. Ulm, *Nanoindentation Analysis as a Two-Dimensional Tool for Mapping the Mechanical Properties of Complex Surfaces*, J. Mater. Res. **24**, 679 (2009).

[53] P. G. Klemens, *Heat Conduction in Solids by Phonons*, Thermochim. Acta **218**, 247 (1993).

[54] S. Li, X. Ding, J. Ren, X. Moya, J. Li, J. Sun, and E. K. H. Salje, *Strain-Controlled Thermal Conductivity in Ferroic Twinned Films*, Sci. Rep. **4**, 6375 (2014).

[55] E. Langenberg et al., *Ferroelectric Domain Walls in $PbTiO_3$ Are Effective Regulators of Heat Flow at Room Temperature*, Nano Lett. **19**, 7901 (2019).

[56] G. Lindgren and C. Canalias, *Domain Wall Conductivity in $KTiOPO_4$ Crystals*, APL Mater. **5**, 076108 (2017).

[57] E. A. Eliseev, A. N. Morozovska, G. S. Svechnikov, P. Maksymovych, and S. V. Kalinin, *Domain Wall Conduction in Multiaxial Ferroelectrics*, Phys. Rev. B **85**, 045312 (2012).

[58] E. K. H. Salje, *Mild and Wild Ferroelectrics and Their Potential Role in Neuromorphic Computation*, APL Mater. **9**, 010903 (2021).

[59] A. Ohashi, M. Kodama, N. Horikawa, and S. Hirai, *Effect of Young's Modulus of Active Materials on Ion Transport through Solid Electrolyte in All-Solid-State Lithium-Ion Battery*, J. Power Sources **483**, 229212 (2021).

[60] S. Zheng, M. Bawazir, A. Dhall, H.-E. Kim, L. He, J. Heo, and G. Hwang, *Implication of Surface Properties, Bacterial Motility, and Hydrodynamic Conditions on Bacterial Surface Sensing and Their Initial Adhesion*, Front. Bioeng. Biotechnol. **9**, 1 (2021).

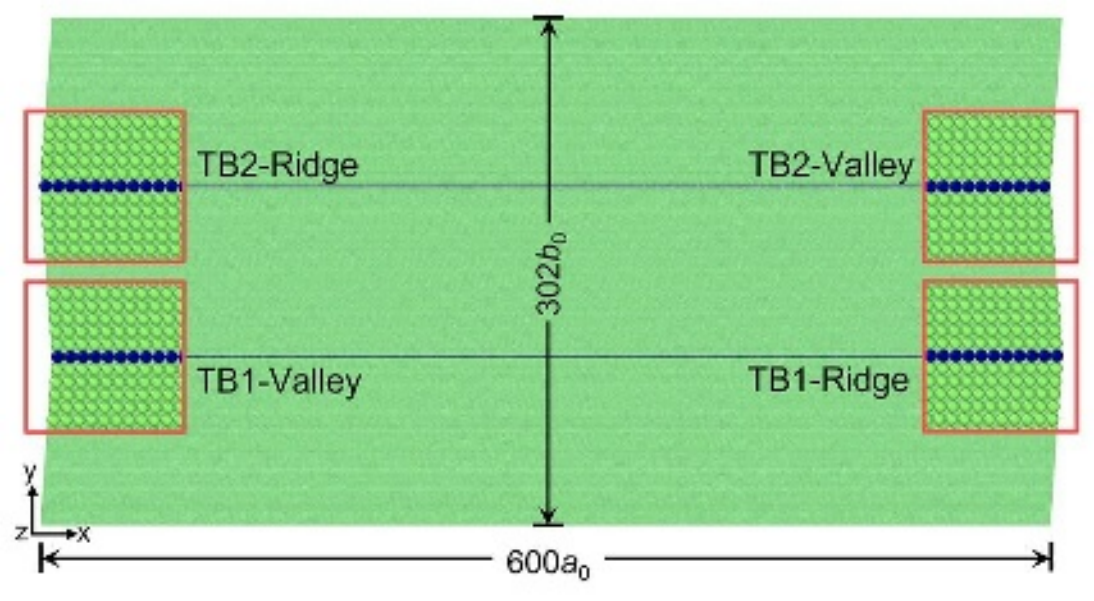
TB2-Ridge
TB2-Valley
$302b_0$
TB1-Valley
TB1-Ridge
y
z
x
$600a_0$

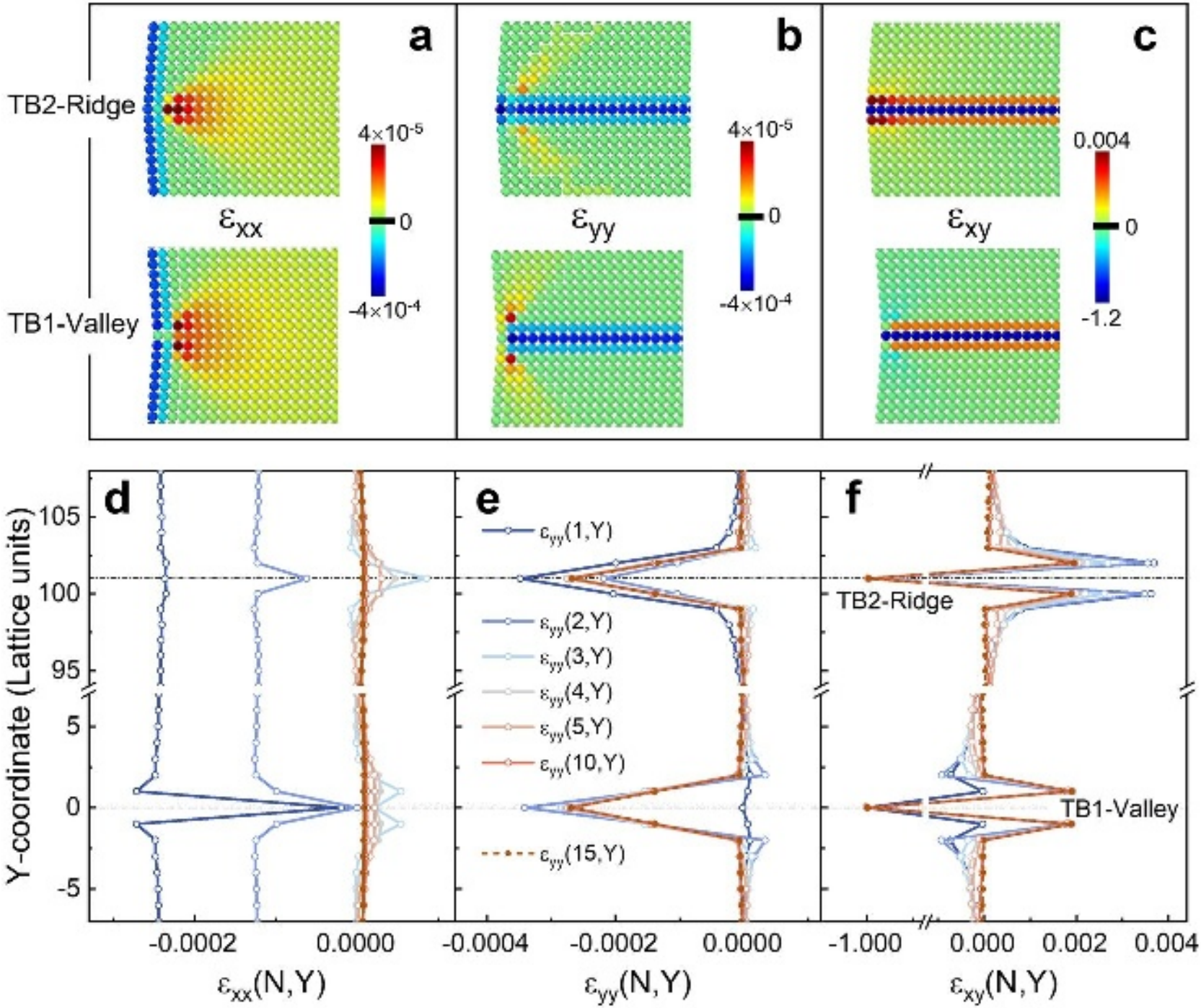
a
b
c
TB2-Ridge
TB1-Valley
ε_{xx}
ε_{yy}
ε_{xy}
4×10⁻⁵
0
-4×10⁻⁴
0.004
-1.2
d
e
f
Y-coordinate (Lattice units)
105
100
95
5
0
-5
ε_{yy}(1,Y)
ε_{yy}(2,Y)
ε_{yy}(3,Y)
ε_{yy}(4,Y)
ε_{yy}(5,Y)
ε_{yy}(10,Y)
ε_{yy}(15,Y)
TB2-Ridge
TB1-Valley
-0.0002
0.0000
-0.0004
-0.0002
0.0000
-1.000
0.000
0.002
0.004
ε_{xx}(N,Y)
ε_{yy}(N,Y)
ε_{xy}(N,Y)

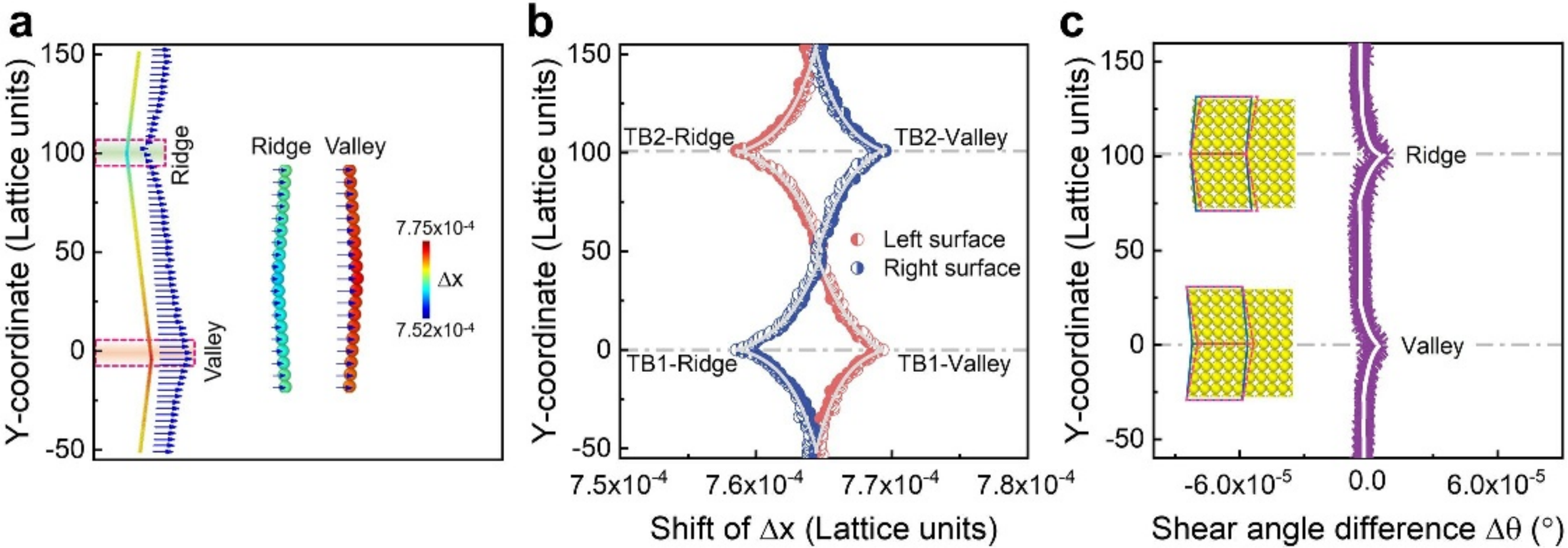
a
b
c
Y-coordinate (Lattice units)
150
100
50
0
-50
Ridge
Valley
Ridge
Valley
7.75x10⁻⁴
Δx
7.52x10⁻⁴
TB2-Ridge
TB2-Valley
TB1-Ridge
TB1-Valley
Left surface
Right surface
7.5x10⁻⁴
7.6x10⁻⁴
7.7x10⁻⁴
7.8x10⁻⁴
Shift of Δx (Lattice units)
-6.0x10⁻⁵
0.0
6.0x10⁻⁵
Shear angle difference Δθ (°)

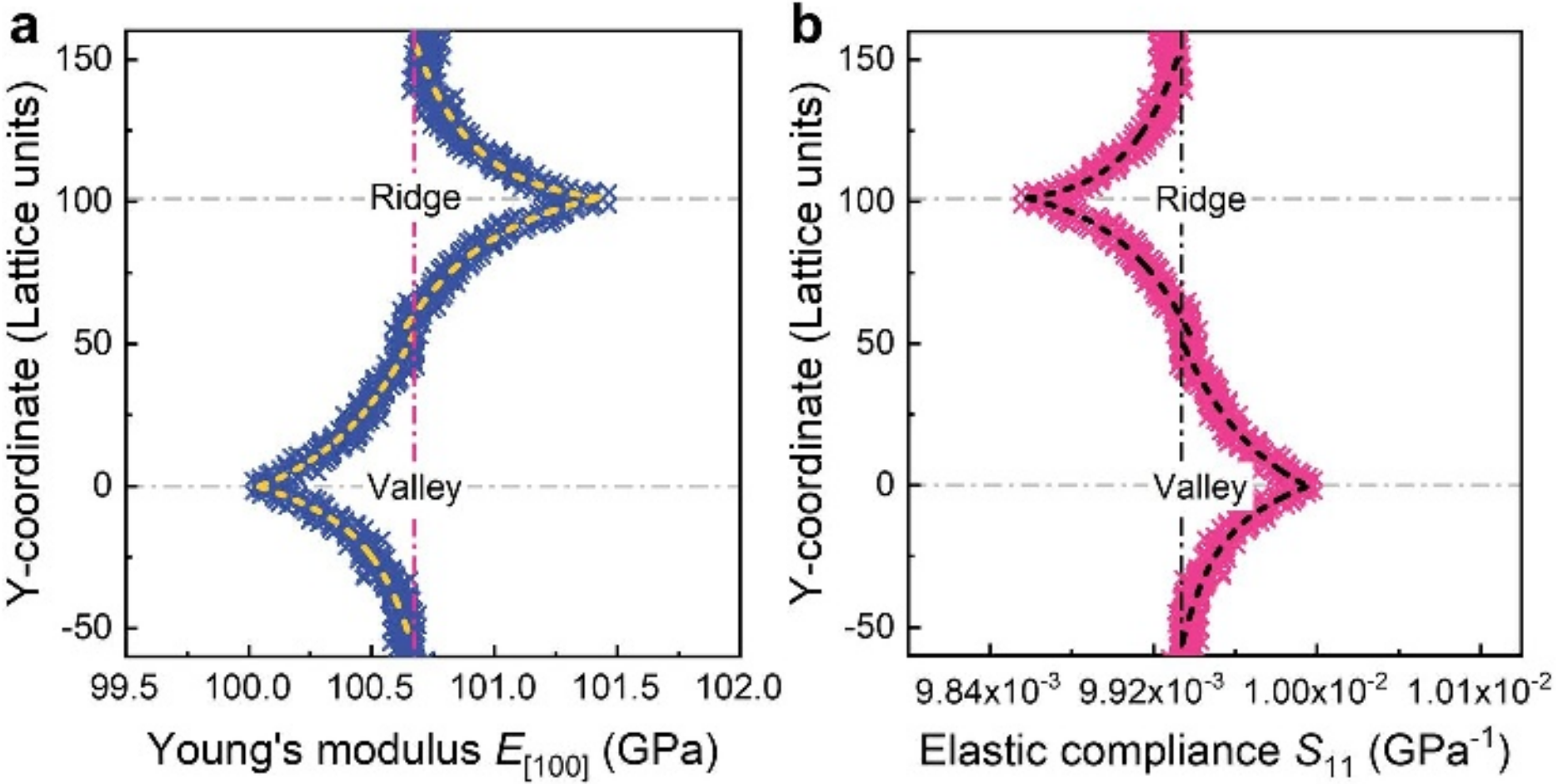
a
150
100
50
0
-50
Y-coordinate (Lattice units)
Ridge
Valley
99.5
100.0
100.5
101.0
101.5
102.0
Young's modulus $E_{[100]}$ (GPa)
b
150
100
50
0
-50
Y-coordinate (Lattice units)
Ridge
Valley
9.84x10^{-3}
9.92x10^{-3}
1.00x10^{-2}
1.01x10^{-2}
Elastic compliance S_{11} (GPa^{-1})